Galaxy And Mass Assembly (GAMA): the 325 MHz radio luminosity function of AGN and star-forming galaxies

Matthew Prescott,[1][*] T. Mauch,[2] M. J. Jarvis,[1,3] K. McAlpine,[1] D. J. B. Smith,[4] S. Fine,[1] R. Johnston,[1] M. J. Hardcastle,[4] I. K. Baldry,[5] S. Brough,[6] M. J. I. Brown,[7] M. N. Bremer,[8] S. P. Driver,[9,10] A. M. Hopkins,[6] L. S. Kelvin,[5] J. Loveday,[11] P. Norberg,[12] D. Obreschkow[9] and E. M. Sadler[13]

[1]*Department of Physics and Astronomy, University of the Western Cape, Private Bag X17, Bellville 7535, South Africa*
[2]*SKA Africa, Third Floor, The Park, Park Road, Pinelands 7405, South Africa*
[3]*Oxford Astrophysics, Denys Wilkinson Building, Keble Road, Oxford OX1 3RH, UK*
[4]*Centre for Astrophysics Research, Science and Technology Research Institute, University of Hertfordshire, Hatfield, Herts AL10 9AB, UK*
[5]*Astrophysics Research Institute, Liverpool John Moores University, IC2, Liverpool Science Park, 146 Brownlow Hill, Liverpool L3 5RF, UK*
[6]*Australian Astronomical Observatory, PO Box 915, North Ryde, NSW 1670, Australia*
[7]*School of Physics and Astronomy, Monash University, Clayton, Victoria 3800, Australia*
[8]*H.H. Wills Physics Laboratory, University of Bristol, Tyndall Avenue, Bristol BS8 1TL, UK*
[9]*ICRAR, University of Western Australia, 35 Stirling Highway, Crawley, WA 6009, Australia*
[10]*SUPA, School of Physics and Astronomy, University of St Andrews, North Haugh, St Andrews KY16 9SS, UK*
[11]*Astronomy Centre, University of Sussex, Falmer, Brighton BN1 9QH, UK*
[12]*Institute for Computational Cosmology, Department of Physics, Durham University, South Road, Durham DH1 3LE, UK*
[13]*School of Physics, University of Sydney, Sydney, NSW 2006, Australia*

ABSTRACT

Measurement of the evolution of both active galactic nuclei (AGN) and star-formation in galaxies underpins our understanding of galaxy evolution over cosmic time. Radio continuum observations can provide key information on these two processes, in particular via the mechanical feedback produced by radio jets in AGN, and via an unbiased dust-independent measurement of star formation rates. In this paper, we determine radio luminosity functions at 325 MHz for a sample of AGN and star-forming galaxies by matching a 138 deg^2 radio survey conducted with the Giant Metrewave Radio Telescope, with optical imaging and redshifts from the Galaxy And Mass Assembly survey. We find that the radio luminosity function at 325 MHz for star-forming galaxies closely follows that measured at 1.4 GHz. By fitting the AGN radio luminosity function out to $z = 0.5$ as a double power law, and parametrizing the evolution as $\Phi \propto (1 + z)^k$, we find evolution parameters of $k = 0.92 \pm 0.95$ assuming pure density evolution and $k = 2.13 \pm 1.96$ assuming pure luminosity evolution. We find that the Low Excitation Radio Galaxies are the dominant population in space density at lower luminosities. Comparing our 325 MHz observations with radio continuum imaging at 1.4 GHz, we determine separate radio luminosity functions for steep- and flat-spectrum AGN, and show that the beamed population of flat-spectrum sources in our sample can be shifted in number density and luminosity to coincide with the unbeamed population of steep-spectrum sources, as is expected in the orientation-based unification of AGN.

Key words: surveys – galaxies: active – galaxies: evolution – galaxies: formation – radio continuum: galaxies.

1 INTRODUCTION

In recent years, it has become apparent that active galactic nuclei (AGN) play an important role in the formation and evolution of

galaxies. Every massive galaxy is now thought to contain a central supermassive black hole that can undergo periods of rapid gas accretion to produce an AGN. The accretion activity of AGN may also have a strong interplay with star formation. Indirect evidence for this comes from comparisons made between the evolution of AGN activity and the star-formation rate of the Universe, which have been

[*]E-mail: mxp@uwcastro.org

shown to follow each other over cosmic history (e.g. Franceschini et al. 1999). In the local Universe, more evidence comes from the correlation between the black hole and bulge masses of galaxies (Kormendy & Richstone 1995; Magorrian et al. 1998). Although more recent results have shown this relationship deviates from being linear when probing lower masses (Graham & Scott 2015), the relationship for more massive galaxies is thought to arise from the regulation of star formation in the bulge due to 'AGN feedback' (for a review, see Fabian 2012). AGN feedback has also been incorporated into semi-analytical models (Bower et al. 2006; Croton et al. 2006), as a way to quench star formation and produce the observed colour bimodality of galaxies (Strateva et al. 2001; Baldry et al. 2004).

The radio source population probed by the current generation of radio surveys probes a mixture of galaxies powered by star formation and AGN activity. At 1.4 GHz flux densities of ~10 mJy and above, the majority of radio sources are radio-loud AGN. Below 10 mJy, there is an increasing number of star-forming (SF) galaxies (Condon 1989). Fanaroff & Riley (1974) found that radio-loud AGN could be subdivided into two types (known as Fanaroff–Riley (FR) types I and II), based on their radio morphologies, which were found to show a division at approximately $L_{178\text{-MHz}} = 10^{25}$ W Hz^{-1}. Those having brighter cores and diffuse lobes are labelled as FR I sources and those with highly collimated jets, which produce 'hot-spots' of high surface brightness at their edges, as FR IIs.

A different classification system based on the presence or absence of narrow emission lines in the optical spectra of radio-loud AGN has also been used over the years (Hine & Longair 1979; Laing et al. 1994; Jackson & Rawlings 1997; Willott et al. 2001). Those with high-excitation emission lines being referred to as High Excitation Radio Galaxies (HERGs) and those without as Low Excitation Radio Galaxies (LERGs). HERGs are the dominant population above $L_{1.4\,\text{GHz}} = 10^{26}$ W Hz^{-1} (Best & Heckman 2012) and are more likely to be associated with the more powerful FR II sources, compared to the LERGs which are more associated with FR Is (although not exclusively). The dichotomy in these populations is believed to be due to two different modes of accretion, with the LERG population undergoing radiatively inefficient accretion of hot gas from the galaxies' interstellar medium and surrounding galaxies, and the HERG population undergoing radiatively efficient accretion of cold gas by mergers and interactions between the host galaxy and gas-rich systems (Allen et al. 2006; Evans et al. 2006; Hardcastle, Evans & Croston 2007; Smolčić et al. 2009; Heckman & Best 2014; Fernandes et al. 2015). Both accretion modes are thought to be important processes in the AGN feedback mechanism. In order to fully understand these different mechanisms, the evolution of these populations has to be determined, usually conducted by either a V/V_{max} analysis or by producing radio luminosity functions (RLFs), whose evolution is parametrized in some way.

It is now established that the most powerful radio-loud AGN (with $L_{1.4\,\text{GHz}} > 10^{25}$ W Hz^{-1}) evolve strongly over the course of cosmic history, with studies finding an increase in their number densities by a factor of 1000 from $z \sim 0$–2 (Longair 1966; Laing, Riley & Longair 1983; Dunlop & Peacock 1990; Willott et al. 2001), which then declines beyond $z \sim 3$ (Shaver et al. 1996; Jarvis & Rawlings 2000; Jarvis et al. 2001; Wall et al. 2005; Rigby et al. 2011). At lower luminosities, however, the picture is much more uncertain.

In an early study by Laing et al. (1983), observations at 178 MHz conducted as part of the 3CRR survey, revealed that sources with $L_{178\,\text{MHz}} < 10^{26}$ W Hz^{-1} exhibit no evolution via a V/V_{max} analysis. Jackson & Wall (1999) also found little or no evolution in the FR I population, compared to FR IIs at frequencies of 151 MHz. The

trend that low-luminosity sources ($L < 10^{25}$ W Hz^{-1}) evolve much less than higher luminosity sources was also seen by Waddington et al. (2001). At 325 MHz, Clewley & Jarvis (2004) found no significant evolution for sources with $L_{325\text{MHz}} < 10^{26.1}$ W Hz^{-1} sr^{-1} out to $z = 0.8$, from matching radio data from the Westerbork Northern Sky Survey (WENSS; Rengelink et al. 1997) with optical Sloan Digital Sky Survey (SDSS) DR1 data and performing a V/V_{max} analysis.

These results are in contrast to those of Brown, Webster & Boyle (2001) who found strong evolution in the low-luminosity radio population at 1.4 GHz out to $z = 0.55$, and by assuming pure luminosity density evolution of the form $L \propto (1 + z)^k$ found $3 < k < 5$ for AGN with $10^{23} < L_{1.4\,\text{GHz}} < 10^{25}$ W Hz^{-1}. Sadler et al. (2007) also found significant evolution for AGN with $10^{24} < L_{1.4\,\text{GHz}} < 10^{25}$ W Hz^{-1} consistent with pure luminosity evolution where $L \propto (1 + z)^{2.0 \pm 0.3}$ from $z = 0.7$, using the 2SLAQ (Cannon et al. 2006) catalogue combined with Faint Images of the Radio Sky at Twenty-Centimeters (FIRST; Becker, White & Helfand 1995) and NRAO VLA Sky Survey (NVSS; Condon et al. 1998).

More recent studies, probing fainter fluxes, have found milder evolution in low-luminosity AGN. Smolčić et al. (2009) produced 1.4 GHz luminosity functions using the VLA-COSMOS survey for AGN with $10^{21} < L_{1.4\text{-GHz}} < 10^{26}$ W Hz^{-1} to $z = 1.3$ and found modest evolution, with $L \propto (1 + z)^{0.8 \pm 0.1}$, or $\Phi \propto (1 + z)^{1.1 \pm 0.1}$, assuming pure luminosity and density evolution, respectively.

McAlpine & Jarvis (2011) found that low-luminosity sources evolve differently from their high-luminosity counterparts out to a redshift of $z = 0.8$ and the measured RLF was found to be consistent with an increase in the comoving space density of low-luminosity sources by a factor of 1.5.

Simpson et al. (2012) using deep $S_{1.4} > 100\,\mu$Jy radio imaging in the Subaru/*XMM–Newton Deep Field*, produced 1.4 GHz luminosity functions divided into the radio-loud and radio-quiet AGN populations. They found that radio-quiet population evolves more strongly than the radio-loud population. Again, very little or no evolution in the number density of the radio-loud AGN with $L_{1.4\,\text{GHz}} \leq 10^{24}$ W Hz^{-1} out to $z = 1.5$ was observed.

Using 1.4 GHz Very Large Array (VLA) data combined with photometric redshifts from the VIDEO survey, McAlpine, Jarvis & Bonfield (2013) found that AGN evolve as $L \propto (1 + z)^{1.18 \pm 0.21}$ at relatively low radio luminosities, assuming pure luminosity evolution.

Finally, using deep from deep (~30 μJy) 1.4 GHz VLA observations of the *Chandra* Deep Field South (CDFS), Padovani et al. (2015) find that the number density of radio-loud AGN evolves as $\propto (1 + z)^2$ out to $z = 0.5$, after which it declines steeply as $\propto (1 + z)^{-4}$.

As well as tracing the population of AGN, radio emission is produced from electrons in the H II regions near massive stars (free–free emission) and cosmic ray electrons produced by supernova remnants (synchrotron emission), and offers a probe of recent star formation in galaxies without the need for an uncertain extinction correction (Condon 1992). It has become well established that the star formation rate of the Universe has declined by a factor of ~10, from $z = 1.0$ to 0.0 (Lilly et al. 1996; Madau et al. 1996; Hopkins & Beacom 2006; Madau & Dickinson 2014). Studies such as Hopkins (2004) for example, incorporated 1.4 GHz measurements into a compilation of star formation indicators to show that the star formation rate in galaxies evolves as $L \propto (1 + z)^{2.7 \pm 0.6}$ for pure luminosity evolution and $\phi \propto (1 + z)^{0.15 \pm 0.6}$ for density evolution. Padovani et al. (2011) also found that SF galaxies evolve as

$L \propto (1 + z)^{2.89 \pm 0.1}$, out to $z = 2.3$, at 1.4 GHz using VLA observations of the CDFS. More recently, McAlpine et al. (2013) measured the 1.4 GHz RLF of SF galaxies, from VLA data combined with photometric redshifts from the VIDEO survey. They measured evolution in the star formation rate density as $L \propto (1 + z)^{2.47 \pm 0.12}$ out to $z = 1$.

In this paper, we present a measurement of the evolution of radio-loud AGN and SF galaxies to $z = 0.5$, by matching a catalogue of radio sources measured at a frequency of 325 MHz from the Giant Metrewave Radio Telescope (GMRT) to their optical counterparts in the Galaxy And Mass Assembly (GAMA) survey. The 325 MHz GMRT survey is the deepest available to date, over a sky area significant enough to alleviate the effects of cosmic variance. The GAMA survey provides reliable spectroscopic redshifts, allowing us to spectroscopically classify AGN and SF galaxies, in addition to providing more accurate redshift and luminosity estimates than studies using photometric redshifts. At present, studies of the evolution in the radio source population made from samples selected at frequencies below 1.4 GHz have primarily relied on radio data with a relatively shallow flux density limit and on photometric redshifts in the optical (e.g. Clewley & Jarvis 2004). Radio-loud AGN samples selected at lower radio frequencies are of interest because the detected population is less dependent on the orientations of the jets. The steep-spectrum lobes of radio galaxies dominate at lower radio frequencies, whereas in the GHz regime the Doppler boosted flat-spectrum cores of pole-on sources are more likely to be detected (Jarvis & McLure 2002).

The structure of this paper is as follows. In Section 2, we outline the GAMA survey and the GMRT data used in this study. In Section 3, we explain the technique to match the radio sources to their optical counterparts. In Section 4, we describe the way we have classified AGN and SF galaxies. In Section 5, we highlight some of the sample properties and show how the spectral indices of the sources vary as a function of luminosity and redshift. In Section 6, we present our RLFs, and determine the evolution in low-luminosity radio sources. We go on to produce RLFs for the HERG and LERG populations, and RLFs for AGN with steep- and flat-spectral indices. In Section 7, we compare our results to other studies. Finally in Section 8, we summarize our main results.

Throughout this paper, we assume $H_0 = 70 \, \mathrm{km \, s^{-1} \, Mpc^{-1}}$, $\Omega_m = 0.3$ and $\Omega_\Lambda = 0.7$.

2 DATA

2.1 Galaxy and mass assembly

GAMA is a multiwavelength (far-UV to radio) survey of ∼290 000 galaxies selected to be complete to $r = 19.8$ mag, combining photometry and spectroscopy from the latest wide-field survey facilities (Driver et al. 2009, 2011; Liske et al. 2015). Covering ∼290 deg² and probing galaxies to $z \sim 0.5$, GAMA allows the study of galaxies and cosmology on scales between 1 kpc and 1 Mpc and provides the link between wide-shallow surveys, such as the SDSS Main Galaxy Sample (Strauss et al. 2002, SDSS MGS) and 2dFGRS (Colless et al. 2001), and narrow-deep surveys such as DEEP2 (Davis et al. 2003), zCOSMOS (Lilly et al. 2007) and VVDS (Le Fèvre et al. 2005).

Optical spectroscopy for the GAMA survey was conducted at the 3.9-m Anglo-Australian Telescope (AAT) using the AAOmega spectrograph (Sharp et al. 2006) on 210 nights, over 6 yr, between January 2008 and September 2014. For further details about spectroscopic target selection and the tiling strategy used for GAMA, the reader is referred to Baldry et al. (2010) and Robotham et al. (2010), respectively. In brief, galaxies are selected for spectroscopy using an input catalogue drawn from the SDSS Data Release 7 (Abazajian et al. 2009) and UKIRT Infrared Deep Sky Survey (UKIDDS; Lawrence et al. 2007). Raw spectra are reduced and calibrated using a pipeline described in Hopkins et al. (2013). GAMA makes extensive use of SDSS photometry, which is obtained for five broad-band filters (*ugriz*) using a dedicated 2.5-m telescope at Apache Point, New Mexico, equipped with a mosaic CCD camera (Gunn et al. 1998) and calibrated with a 0.5 m telescope (Hogg et al. 2001). For greater detail regarding the SDSS, the reader is referred to York et al. (2000) and Stoughton et al. (2002).

In the following analysis, we use imaging data for galaxies which make up the *r*-band limited Main Survey, observed in three $12 \times 5 \, \mathrm{deg}^2$ GAMA fields located along the celestial equator at 9, 12 and 14.5 h (known as G09, G12 and G15). In order to measure the RLF and its evolution, we select galaxies from GAMA TilingCat43 with redshifts between $0.002 < z < 0.6$, $nQ \geq 3$, $r \leq 19.8$ mag and a Survey Class ≥ 4 which ensures we are using reliable redshifts and have a well-defined selection limit in which we are >98 per cent complete. This results in a sample of 185, 125 galaxies over G09, G12 and G15.

2.2 GMRT data

The 325 MHz radio survey covering the GAMA fields, using the GMRT, is fully described in Mauch et al. (2013).[1] A total of 212, 15 min pointings were observed over eight nights in January 2009, three nights in May 2010 and one night in June 2010. These pointings overlap with 138 deg² of the GAMA G09, G12 and G15 regions. Flagging, calibration, self-calibration and source detection of each pointing was conducted using a pipeline making use of the AIPS software package. After reduction, the pointings in each field were mosaicked, producing images with resolutions of 14, 15 and 23.5 arcsec with minimum rms noises of ∼0.8 , ∼1 and ∼1.5 mJy beam⁻¹, for fields G09, G12 and G15, respectively. A source catalogue was produced by fitting elliptical Gaussians in the mosaics, which resulted in a final catalogue that contains 5264 sources. To remove spurious detections, we limited the GMRT catalogue to include only sources brighter than 5σ (Peak flux density/local rms ≥ 5), resulting in a catalogue of 4931 radio sources.

3 GAMA/GMRT CROSS-MATCHING

Cross-matching between the GAMA and the GMRT catalogues was conducted by visual inspection of radio contours on to optical images. This was done because the elliptical Gaussian model fitted to GMRT radio sources is insufficient to describe the wide range of source morphologies at the resolution of the survey and the Gaussian fits are also sometimes affected by image artefacts. Automated cross-matching of the catalogues based on position separation will be unable to take account of these errors. We treat the cross-matching of single and multiple component radio sources separately, where radio sources within a radius of 50 arcsec of each other are considered as being potential multiple component sources. Sources with no other radio source within 50 arcsec are treated as

---

[1] See also http://www.extragalactic.info/mjh/gmrt/

single component sources. Using this method, we are considering every potential optical counterpart from GAMA within 50 arcsec of a GMRT radio source.

3.1 Single component sources

There are 3616 single component radio sources (i.e. sources with no other radio source within 50 arcsec) in the GMRT catalogue. In order to find optical counterparts, each radio source is matched to the nearest object in the selected GAMA spectroscopic catalogue with a maximum offset of 15 arcsec. Contour maps of each GMRT source were then produced and overlaid on top of a 3 arcmin × 3 arcmin SDSS *r*-band images of the potential counterpart, and inspected to establish whether the radio source has a robust optical counterpart. Visual inspection was performed by two of us to ensure its reliability. As a double-check to ensure the GMRT identifications were real, contour maps from the 1.4 GHz surveys FIRST and NVSS, where available, were also overlaid on the SDSS image. The FIRST and NVSS contours complement the GMRT data when matching, as FIRST provides resolved (6.4 arcsec × 5.4 arcsec resolution in the GAMA regions) detections of the sources and the NVSS, despite its lower resolution of 45 arcsec, has greater surface brightness sensitivity.

Of the 3616 single component sources, we found 573 lie within 15 arcsec of a GAMA source in the selected spectroscopic catalogue. We then visually matched 370 out of these GMRT sources with their optical counterparts in GAMA.

For comparison, we also looked for single component counterparts using the likelihood ratio technique (Sutherland & Saunders 1992; Smith et al. 2011; McAlpine et al. 2012). This resulted in 330 GAMA/GMRT matches with reliabilities >0.8. This method resulted in fewer matches overall, mainly due to the non-trivial structure of many radio sources at the GMRT resolution (e.g. McAlpine et al. 2012), so we use our visually classified sample for the rest of this paper. At present, visual classification is acknowledged as being the most reliable method of cross-matching radio source catalogues with optical data sets (e.g. Fan et al. 2015).

3.2 Multiple component sources

To find the counterparts of multiple component sources (i.e. radio sources with a radio counterpart within 50 arcsec), GMRT contour maps of all radio sources were again overlaid with FIRST and NVSS contours, on top of a 5 arcmin × 5 arcmin SDSS *r*-band image of the nearest GAMA object. Visual inspection of candidate multiple component radio sources was performed in the same way as was done for single component sources.

From the initial GMRT catalogue of 4931 5σ radio source components, we found 757 potential multiple component sources. After inspection, we identified 84 multiple component radio sources, together with a further 46 objects that turned out to be separate single component sources near unrelated GMRT sources that could not be matched (bringing the total number of single component sources to 414). The flux densities of multiple component objects are simply the sum of the flux density of each individual component in the GMRT catalogue.

Fig. 1 shows an example of one of the GAMA/GMRT matches, GAMAJ085701.76+013130.9, with the SDSS *r*-band image overlaid with radio contours from the GMRT (blue), FIRST (yellow) and NVSS (red). At *z* = 0.27, this galaxy has a projected size of ∼1.3 Mpc and is a previously undiscovered Giant Radio Galaxy
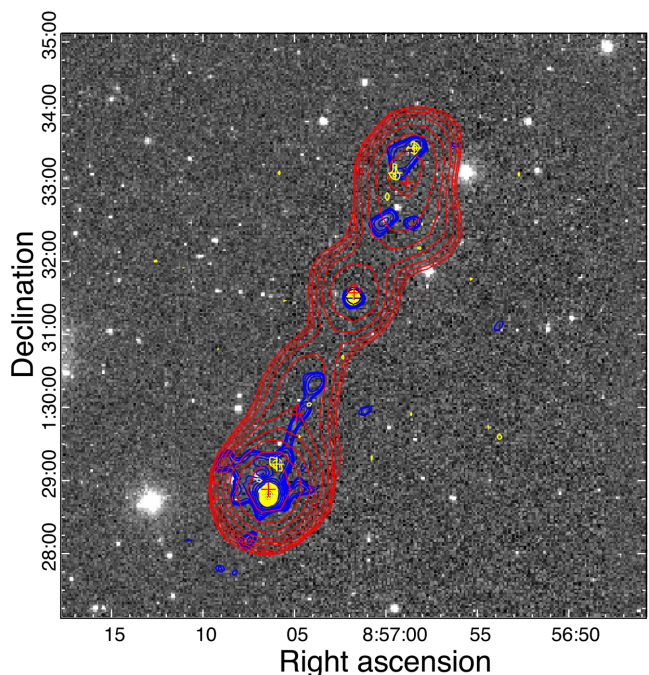
Figure 1. An example of one of the GMRT/GAMA matches GAMAJ085701.76+013130.9, showing the SDSS *r*-band image, overlaid with radio contours from the GMRT (blue), FIRST (yellow) and NVSS (red). At *z* = 0.27, the FR II AGN has a projected size of 1.3 Mpc, making it a previously undiscovered GRG.

(GRG; Schoenmakers et al. 2001; Saripalli et al. 2005). Automated methods such as the likelihood ratio technique in this case would be able to match the core of the radio source to an optical counterpart, but would incorrectly match the lobes to some other optical source, if considered separately.
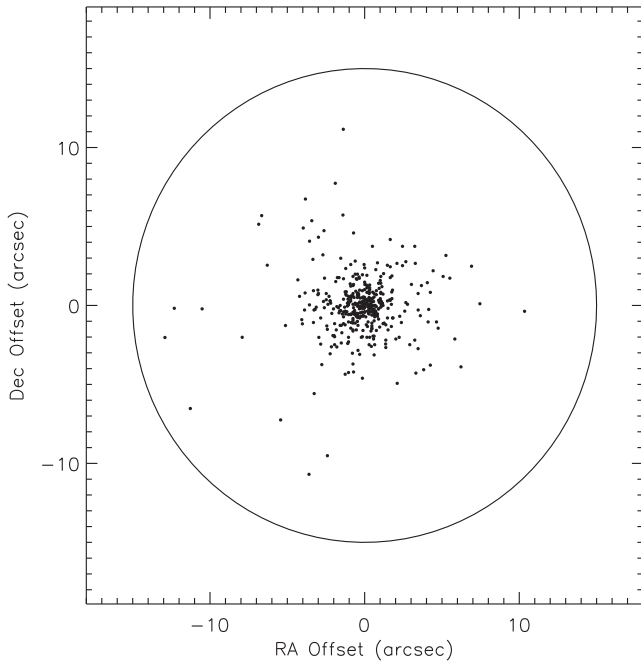
3.3 Positional offsets

Fig. 2 shows the positional offsets between the GAMA and GMRT positions of the 414 single component sources. The median positional offset between the coordinates is found to be 1.51 arcsec.

To test our matching process, in Fig. 3 we show the distribution of the positional offsets between each of the 185 125 GAMA sources and the 4931 GMRT sources (blue-dashed line). Here, this is compared to the positional offsets between the mean of 10 GAMA catalogues with randomized positions and again matched to the nearest GMRT source (black solid line). The curves converge at a separation of 15 arcsec, which implies that genuine GMRT/GAMA matches should all lie with 15 arcsec of one another.

Integrating both curves out to 15 arcsec, yields 778 matches between the real GAMA/GMRT catalogues and 267 matches between the random/GMRT catalogue which indicates 511 genuine GAMA/GMRT matches are expected, which is consistent with our final sample of 499 (414 single and 84 multiple component) GAMA/GMRT matches.

We find that ∼10 per cent (499/4 931) of the radio sources are matched to GAMA. This is a higher fraction than other matched radio/optical samples with similar radio flux density limits, for example Sadler et al. (2002) and Mauch & Sadler (2007) find that ∼1–2 per cent of NVSS radio sources are detected in the 2dFGRS and 6 degree Field Galaxy Survey (6dFGS; Jones et al. 2004). This

Figure 2. The positional offsets between the GAMA and GMRT for the 414 single component matches out to $z = 0.6$. The circular line represents a radius of 15 arcsec.
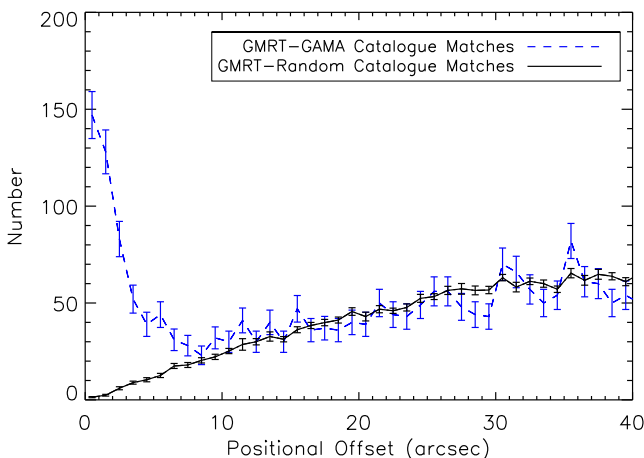
Figure 3. Histogram displaying the positional offset between each of the 185 125 GAMA sources in the spectroscopic catalogue, with $z < 0.6$ and $nQ \geq 3$ and $r \leq 19.8$, matched to the nearest of the 4931 5σ GMRT sources within 3 arcmin (blue-dashed line). This is compared to the positional offsets between the mean of 10 random GAMA catalogues matched to the nearest GMRT source (black solid line).

is due to the fainter optical limits of GAMA, which probes a larger range of redshifts.

4 SOURCE CLASSIFICATION

After matching the optical/radio counterparts, we divided our sample into AGN and SF galaxies, by inspecting their individual optical spectra, in a similar fashion to Sadler et al. (2002) and Mauch & Sadler (2007). AGN can have spectra with either pure absorption

features like that of an elliptical galaxy, broadened emission features (known as type I AGN), strong nebular emission [O II], [O III] and [N II] lines compared to the Balmer series (known as type II AGN), or spectra with absorption lines with weak narrow emission lines [low-ionisation nuclear emission line regions (LINERs)]. In this work, sources with optical spectra revealing strong narrow emission lines consistent with H II regions, were classified as being SF galaxies. Examples of spectra for AGN and SF galaxies can be seen in Fig. 4. The spectrum for each object was inspected independently by three people to ensure that each classification was reliable and subsequently double-checked with the AGN/SF Kewley et al. (2001) classifications, if it was available in GAMA's emission line catalogue.

From the sample of 499 GAMA/GMRT matches out to $z = 0.6$, we classified 453 sources as AGN and 45 as SF galaxies. Upon further inspection, one source, GAMA J142831.94+014331.4, was found serendipitously to be an F5 type radio star in the catalogue of Kimball et al. (2009).

5 SAMPLE PROPERTIES

Each source in our GAMA/GMRT catalogue was detected by the NVSS and we assigned an NVSS identification (and 1.4 GHz flux density) during the visual cross-matching process. In order to determine radio luminosities of each object, we k-correct the observed flux densities assuming $S_\nu \propto \nu^\alpha$ and use spectral indices determined from the ratios between the 325 MHz and 1.4 GHz fluxes retrieved from the NVSS catalogue.
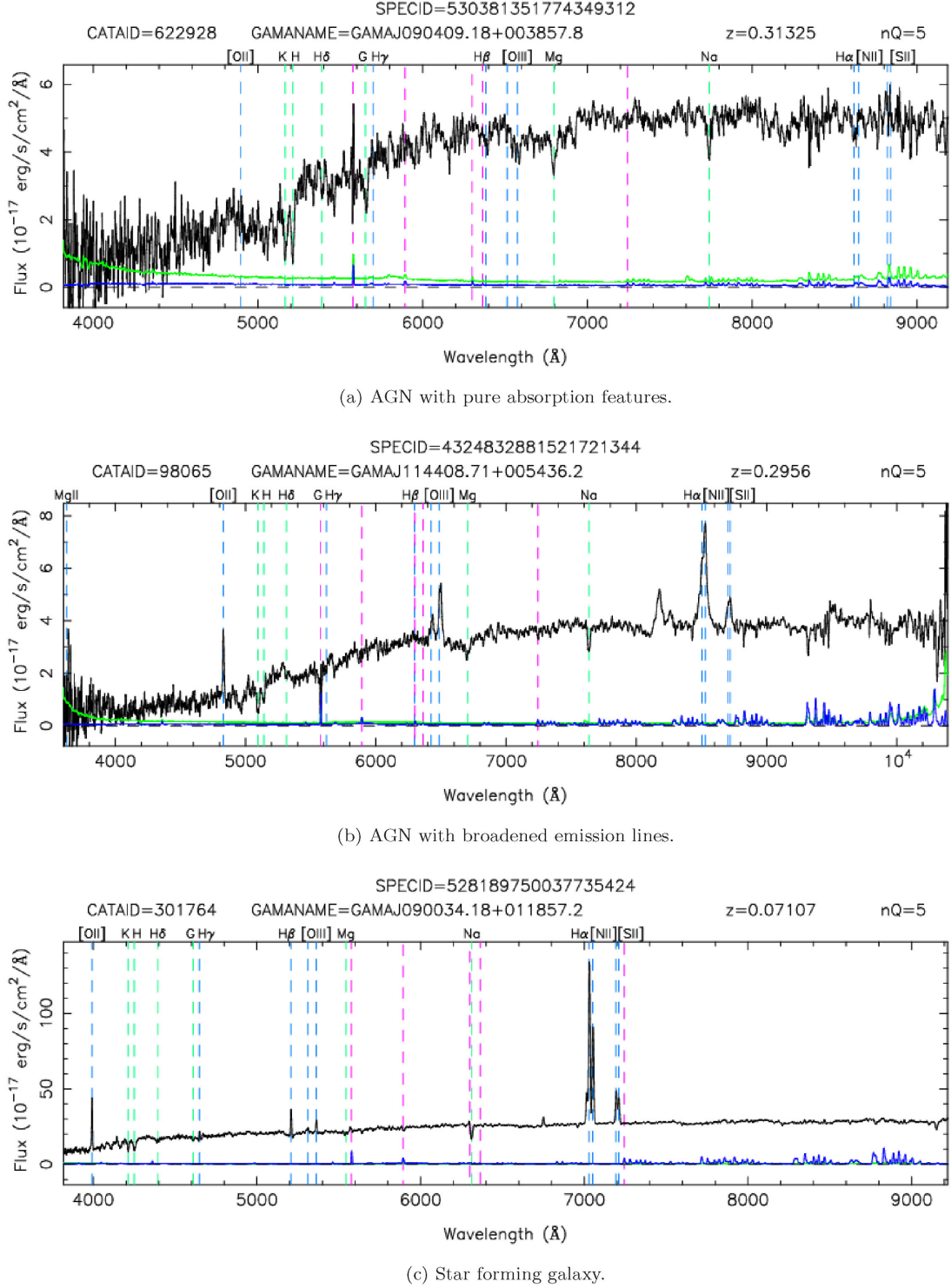
Median redshifts were found to be $z = 0.36$ for the AGN, and $z = 0.06$ for the SF galaxies. In Fig. 5 and Fig. 6, we show the redshift distribution histogram and the redshift versus radio luminosity plane, respectively, for both the AGN and SF galaxies. These figures illustrate that SF galaxies become the dominant population of radio sources in the local Universe ($z < 0.1$) at the limit of ~10 mJy at 325 MHz.

5.1 Spectral indices

Given that every 325 MHz GMRT source has a detection at 1.4 GHz from the NVSS, we can investigate the spectral index distribution for both SF galaxies and AGN. Fig. 7 shows the distribution of the spectral indices across the whole sample. We find that the median spectral indices for AGN and SF galaxies are $\alpha = -0.68 \pm 0.22$ and -0.82 ± 0.28, respectively, which agree well with values reported by Mauch et al. (2003), Owen et al. (2009), Mauch et al. (2013), Randall et al. (2012), Smolčić et al. (2014) and Coppejans et al. (2015).

Fig. 8 shows how the spectral indices of AGN and SF galaxies vary as a function of redshift. In the past, steep-spectral indices have been used to select high-redshift radio galaxy candidates from low-frequency radio surveys (e.g. De Breuck et al. 2001; Jarvis et al. 2001; Cruz et al. 2006); however, we find that there is no significant steepening of the spectral index in our sample with redshift, albeit over a relatively low redshift range. This trend was also found by Smolčić et al. (2014) out to $z = 2.5$, in a 325 MHz VLA survey of the COSMOS field.

In Fig. 9, we show the spectral indices as a function of luminosity. Although there is large scatter in the data, we find there is a slight decrease in spectral index with increasing luminosity for the AGN. This decrease may arise due to an increasing contribution from higher luminosity FR II sources whose emission will be dominated by steep-spectrum optically thin lobes. A straight line of the best fit

(a) AGN with pure absorption features.

(b) AGN with broadened emission lines.

(c) Star forming galaxy.

Figure 4. Example optical spectra found in our GAMA/GMRT matched sample (black lines). Also plotted is the 1σ error (green lines) and sky (blue). AGN are classified as having either pure absorption features (a) or broadened emission features (b). A spectrum of a typical SF galaxy that have strong, narrow, emission lines such as Hα can be seen in (c).

to the AGN data points yields a gradient of $m = -0.077 \pm 0.022$ and constant of $c = 1.23 \pm 0.55$. A Spearman Rank correlation test gives a coefficient of $\rho = -0.229$ with a significance of the deviation from zero of 1.02×10^{-6}, indicating a weak but significant correlation.
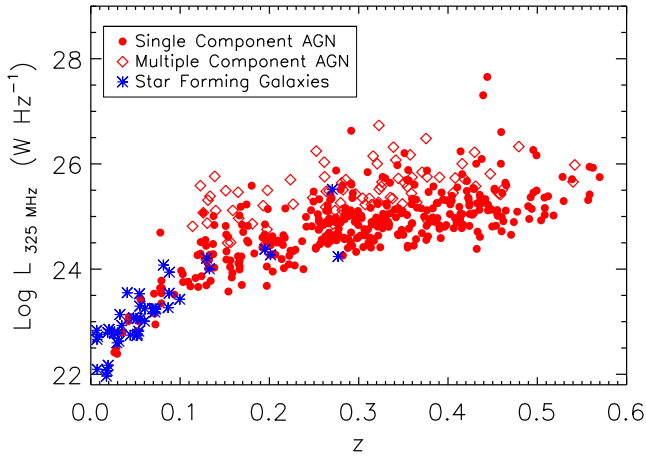
6 RADIO LUMINOSITY FUNCTIONS

6.1 Measuring the RLF

To measure the cosmic evolution of the radio sources, we determine the RLFs for different redshift slices using the $1/V_{\mathrm{max}}$ method,
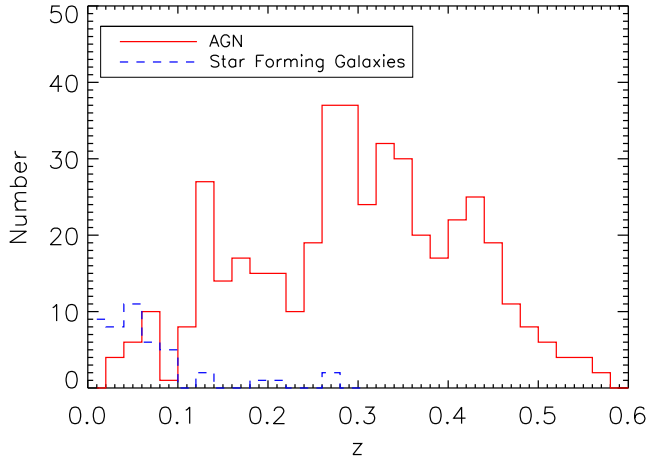
Figure 5. Redshift distribution of GAMA–GMRT-matched AGN (solid red line) and SF galaxies (dashed blue line). The median redshift for the AGN is $z = 0.36$, and 0.06 for the SF galaxies.


Figure 6. The luminosity–redshift distribution of the matched GAMA–GMRT sources, showing single component AGN (red-filled circles), multiple component AGN (red diamonds), and SF galaxies (blue stars). SF galaxies become the dominant radio sources at $z < 0.1$ at the limits of the GMRT survey.
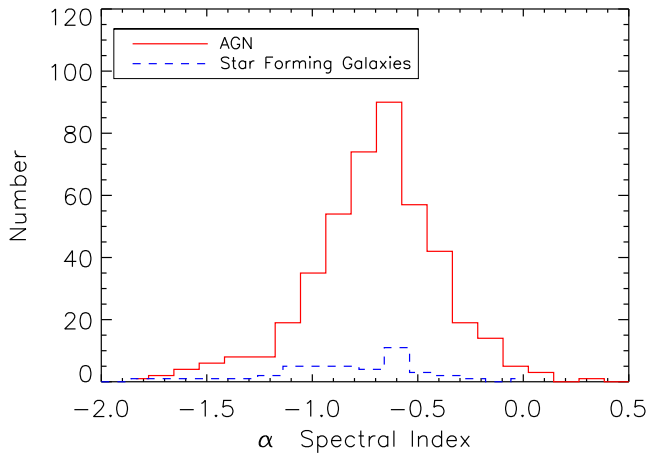
Figure 7. The spectral index distribution for AGN (red, solid line) and SF galaxies (blue, dashed line). The spectral indices of the sources are calculated from the ratios between 325 MHz GMRT and 1.4 GHz NVSS flux densities.
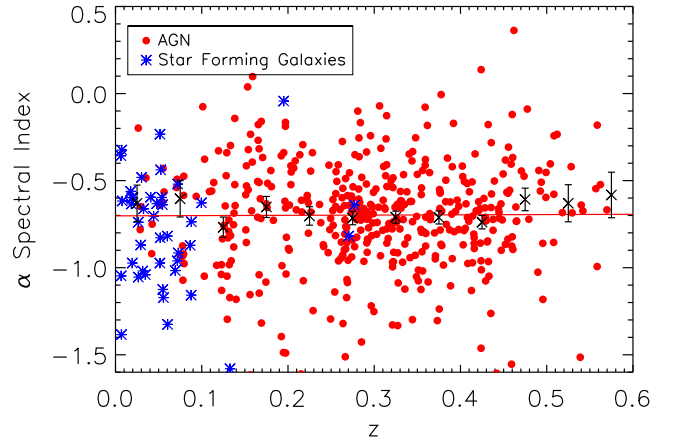
Figure 8. The spectral index distribution for AGN (red dots) and SF galaxies (blue stars) as a function of redshift. The black crosses and error bars indicate the mean and standard error on the mean of the spectral index for the AGN in bins of $\Delta z = 0.05$. The red line shows the line of the best fit for the AGN data points. The average spectral indices remains more or less constant with increasing redshift.
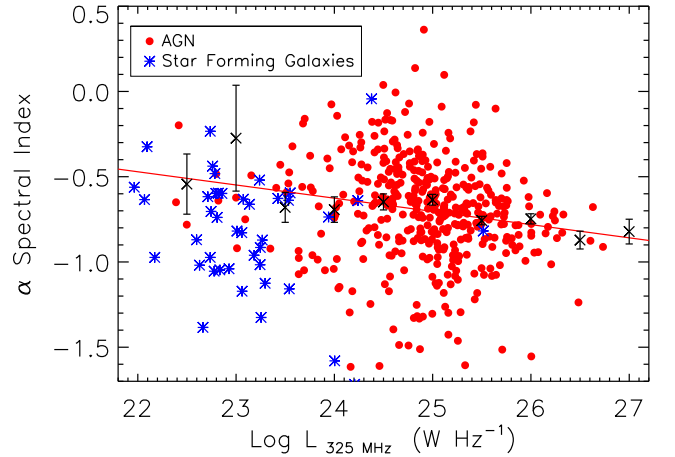
Figure 9. The spectral index distribution for AGN (red dots) and SF galaxies (blue stars) as a function of luminosity. The red solid line shows the line of the best fit for the AGN data points. The black crosses and error bars indicate the mean and standard error on the mean of the spectral index for the AGN in bins of $\Delta \log_{10}(L_{325})$ W Hz^{-1} = 1. There is a slight decrease in the spectral index with increasing luminosity.

where V_{max} is the maximum comoving volume within which a galaxy could lie within a redshift slice and within the flux limits of the survey (Schmidt 1968). The RLF for a given luminosity bin is given by

$$\Phi_z(L) = \sum_{i=1}^{N} \frac{1}{C_i \times V_{\mathrm{max,i}}}. \tag{1}$$

Here, C_i is the completeness of the survey. We determine upper and lower 1σ Poisson confidence limits using the approximation prescribed in Gehrels (1986). As our sample is a matched radio/optical sample, we have to take into account both the optical and radio limits of the surveys, where V_{max} is the taken as the minimum from the optical and radio V_{max} for each source:

$$V_{\mathrm{max}} = \min(V_{\mathrm{max,radio}}, V_{\mathrm{max,optical}}). \tag{2}$$
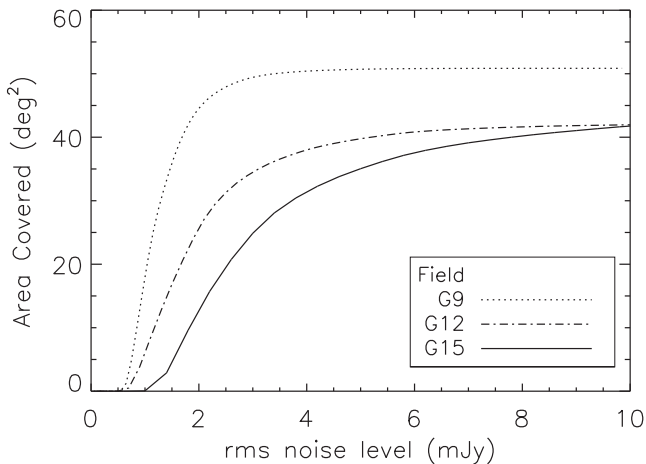
Figure 10. Figure showing the cumulative area as a function of rms noise level, for each of the three GAMA regions. The total areal coverages for G09, G12 and G15 are 50.9, 42.3 and 45.0 deg^2, respectively.
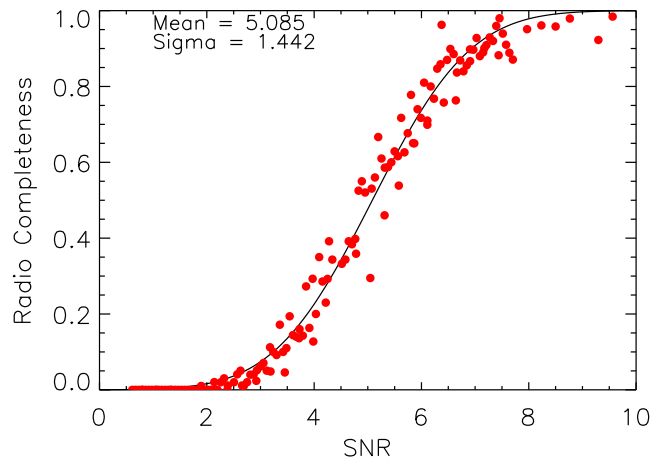

Figure 11. Radio completeness as a function of the signal-to-noise ratio. Red data points show the fraction of simulated sources detected in the GMRT images fitted with a cumulative distribution function (black line). In this study, we only use sources with an SNR $\geq$ 5, and so $C_R > 0.5$ for each source.

$V_{\mathrm{max,\,optical}}$ was computed from $z_{\mathrm{max,\,optical}}$, the maximum redshift in which a galaxy can be observed, calculated via Spectral Energy Distribution (SED) fitting of the optical spectra described fully in Taylor et al. (2011). As the GMRT mosaics have non-uniform sensitivity, the effective area of the survey changes as a function of the flux limit. The volume of space available to a source of a given luminosity $L(V_{\mathrm{max,\,radio}})$ has to be calculated by taking into account the variation of survey area as a function of flux density limit. Fig. 10 shows how the cumulative area of the survey varies as a function of rms noise for each of the GMRT mosaics covering G09, G12 and G15. We use the same method of calculating $V_{\mathrm{max,\,radio}}$ described in Smolčić et al. (2009). First, the differential area in the survey in small bins of rms noise is determined for each field from Fig. 10. To calculate $V_{\mathrm{max,\,radio}}$ for a radio source with luminosity L, we compute the maximum redshift ($z_{\mathrm{max,\,i}}$) that the source would have in each differential rms bin i across the three survey fields. $z_{\mathrm{max,\,i}}$ is the redshift the source would have before it drops out of the survey at five times the rms of the bin i. $V_{\mathrm{max,\,radio}}$ for the source is then just the sum of all of the individual $V_{\mathrm{max,\,radio,\,i}}$ normalized by the survey area of that rms bin A_i:

$$V_{\mathrm{max,radio}} = \sum_{i=1}^{n} F_i \times V_{\mathrm{max,radio,i}}(z_{\mathrm{max,i}}), \qquad (3)$$

where F_i is the fraction of sky corresponding to the area in the bin i, and the sum is over all bins in each of the three fields.

The completeness, C_i, in equation (1) for the RLFs is a combination of the redshift success and a radio completeness ($C_i = C_{\mathrm{redshift\,success}} \times C_R$). The redshift success is defined as the number of sources with a reliable redshift determination ($NQ \geq 3$) divided by the total number of sources in the input catalogue within a given r-band fibre magnitude. In Loveday et al. (2015), the redshift success is shown to be well fitted by a modified sigmoid function (see their equation 1) which we apply here. The GAMA survey is highly complete and has a redshift success of 99 per cent at $r_{\mathrm{Petro}} = 19.2$ and 96 per cent at the survey limit of $r_{\mathrm{Petro}} = 19.8$ (see Liske et al. 2015 for more details).

Errors in fitting fainter sources in the GMRT catalogue can cause it to be incomplete near the radio survey limit. We have derived the completeness as a function of signal to noise for the GMRT catalogue by inserting 6000 simulated sources over a range of flux

densities at random positions into three images from the survey, one from each of the G09, G12 and G15 fields. We then used the same source finding procedure outlined in section 4 of Mauch et al. (2013) to detect the simulated sources. Fig. 11 shows the fraction of simulated sources detected in the GMRT images (i.e. the completeness) as a function signal-to-noise ratio. We have fitted the data with the cumulative distribution function:

$$C_R = 0.5 \left[1 + \mathrm{erf}\left(\frac{\mathrm{SNR} - \mu}{\sqrt{2}\sigma} \right) \right], \qquad (4)$$

where C_R is the radio completeness correction, SNR is the local signal-to-noise ratio, $\mu = 5.1$ and $\sigma = 1.4$.

6.2 SF galaxies

The 325 MHz RLF for SF galaxies between $0.002 < z < 0.1$ for our sample can be seen in Fig. 12 (and Table 1). The sample is truncated at $z < 0.1$ to minimize the effects of evolution. The shape of the RLF
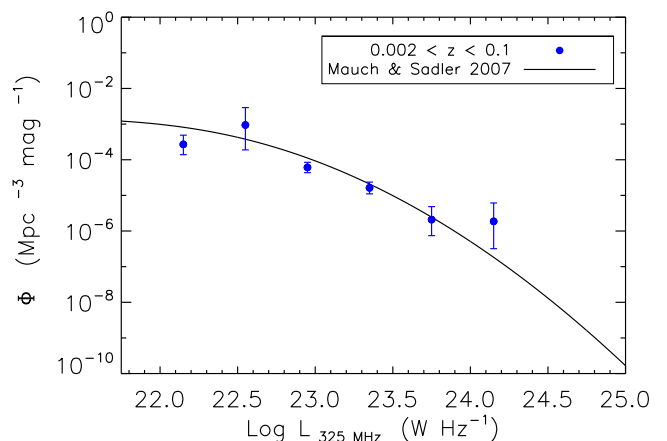
Figure 12. The 325 MHz RLF for SF in the redshift range $0.002 < z < 0.1$ shown in blue. This is compared to the local RLF of Mauch & Sadler (2007), which has converted to 325 MHz from 1.4 GHz assuming a spectral index of $\alpha = -0.7$, shown in black. Error bars are determined using the prescription of Gehrels (1986).

Table 1. The 325 MHz RLF for SF galaxies.

Luminosity ($\log_{10}(L_{325MHz})$)	Number density (Mpc^{-3} mag^{-1})	Number
22.15	$2.72^{+2.22}_{-1.32} \times 10^{-4}$	4
22.55	$1.00^{+2.11}_{-0.81} \times 10^{-3}$	7
22.95	$6.10^{+2.36}_{-1.76} \times 10^{-5}$	14
23.35	$1.63^{+0.73}_{-0.53} \times 10^{-5}$	10
23.75	$2.09^{+2.75}_{-1.35} \times 10^{-6}$	2
24.15	$1.86^{+4.26}_{-1.54} \times 10^{-6}$	1
Total		38

is broadly consistent with the local RLF of Mauch & Sadler (2007) converted to 325 MHz from 1.4 GHz assuming a spectral index of $\alpha = -0.7$. One key difference between these surveys is the short baseline coverage that allows extended sources to be recovered in the study of Mauch & Sadler (2007), whereas such sources may be missed in the GMRT survey. We therefore may not be sensitive to such extended sources, and our measured RLF should be treated as a lower limit.

Assuming synchrotron self-absorption becomes important in SF galaxies, at lower frequencies we would expect a population of flatter spectrum sources to shift the median spectral index above $\alpha = -0.7$. In Fig. 9, we see no significant population of flat spectrum sources in the SF population, which, assuming synchrotron self-absorption means we are likely to be missing sources in the flux density range of the SF galaxies. These may be missing due to resolution bias; i.e. they have a peak flux density below the survey limit, but their total flux density would be above the limit, if they were detected. This may even be occurring at the relatively low resolution and surface brightness sensitivity of the GMRT data.

No evolution measurement is possible from our data, as only six SF galaxies are detected above $z = 0.1$, with the majority actually at $z < 0.1$ (Fig. 5). It is evident we are missing the faintest SF galaxies with $\log_{10}L_{325} < 22.0$. To rectify this, deeper radio data with μJy flux limits, over the same area of sky, would be needed to further constrain the faint-end of the luminosity function at frequencies of 325 MHz. Indeed, this is one of the key science cases for current and future deep radio surveys covering much smaller areas (Jarvis et al. 2014; McAlpine et al. 2015).

With these caveats in mind, we can derive a lower limit of the local star formation rate density, using the 1.4 GHz luminosities of the galaxies and converting them to star formation rates (in M$_\odot$ yr^{-1}) via the relation presented in Bell (2003), we estimate the total star formation rate density as $\rho_{SFR} = \Sigma(SFR/V_{max}) = 0.013 \pm 0.002$ M$_\odot$ yr^{-1} Mpc^{-3}.

Many different estimators have been used to determine the star formation rate density of the Universe. At 1.4 GHz, Mauch & Sadler (2007) find the star formation rate of the local Universe to be $\rho_{SFR} = 0.022 \pm 0.001$ M$_\odot$ yr^{-1} Mpc^{-3}, which is slightly greater than our result. Using Hα measurements, Gunawardhana et al. (2013) have also estimated the evolution of the star formation density out to $z < 0.34$. Using values from their table 3, $\rho_{SFR} = 0.024 \pm 0.006$ M$_\odot$ yr^{-1} Mpc^{-3} between $0 < z < 0.24$. Westra et al. (2010) using data from the Smithsonian Hectospec Lensing Survey measured a value of $\rho_{SFR} = 0.018$ M$_\odot$ yr^{-1} Mpc^{-3} out to $z < 0.2$. James et al. (2008) found the star formation density of local SF galaxies to lie between $\rho_{SFR} = 0.016$ and $\rho_{SFR} = 0.023$ M$_\odot$ yr^{-1} Mpc^{-3} from a sample of galaxies in the Hα Galaxy Survey.

6.3 AGN

The RLFs for AGN in two redshift slices ($0.002 < z < 0.25$ and $0.25 < z < 0.5$) are shown in Fig. 13 (See Table 2 for the RLF values). We find that the 325 MHz RLF at these redshifts is comparable to the local 1.4 GHz RLF of Mauch & Sadler (2007) converted to 325 MHz assuming a spectral index of $\alpha = -0.7$. There also appears to be evidence for positive evolution, at least at $L_{325} > 10^{25}$ W Hz^{-1}.

In order to quantify the cosmic evolution of the AGN, following Dunlop & Peacock (1990), we fit a double power law function to the data given by

$$\Phi(L) = \frac{C}{(L_*/L)^A + (L_*/L)^B}, \tag{5}$$

where C is the normalization, L_* is the luminosity corresponding to the break in the RLF and A and B are the bright and faint end slopes. We simultaneously fit both redshift slices for evolution assuming two scenarios for the RLF, one in which the luminosity of the radio sources is fixed and undergoes pure density evolution parametrized by

$$\Phi_z(L) = (1 + z)^k \Phi_0(L), \tag{6}$$

and another in which the number density of radio sources is fixed and the population undergoes pure luminosity evolution:

$$\Phi_z(L) = \Phi_0 \left(\frac{L}{(1+z)^k} \right), \tag{7}$$

where $\Phi_z(L)$ is the RLF at redshift z, $\Phi_0(L)$ the normalization of the local RLF, and k denotes the strength of the evolution.

Fig. 13 shows the best fits for both evolution scenarios. We fit these assuming both a fixed and variable bright and faint-end slopes of the RLF. For the fixed slopes, we use those found in the local 1.4 GHz luminosity function of Mauch & Sadler (2007), with $A = 1.27$ and $B = 0.49$. The parameter values obtained from the fits are shown in Table 3.

We find evidence of mild evolution in the AGN RLF. Evolution parameters of $k = 0.92 \pm 0.95$ in the case of pure density evolution and $k = 2.13 \pm 1.96$ for pure luminosity evolution, are obtained without fixing the faint and bright-end slopes. Fixing the slopes to the values found by Mauch & Sadler (2007), we find $k = 1.51 \pm 0.92$ for pure density evolution and $k = 2.75 \pm 1.51$ for pure luminosity evolution. The values of the bright-end slopes we find when fitting for all the parameters are steeper than those found by Mauch & Sadler (2007), but the faint-end slope is very similar. L_* and C are similar in all the fits, with $\log_{10}(L_* \approx 26.25$ W Hz$^{-1})$ and the normalization $C \approx -6.5$ Mpc^{-3} in all cases.

We also fit straight lines of the best fit to the AGN data for the whole range of luminosities and those with $\log_{10}L_{325} < 24.5$ W Hz^{-1}, which have the form in the case of pure density evolution:

$$\log_{10} \Phi_z = m \log_{10} L + k \log_{10}(1 + z) + c, \tag{8}$$

and in pure luminosity evolution:

$$\log_{10} \Phi_z = m(\log_{10}(L) - k \log_{10}(1 + z)) + c. \tag{9}$$

These fits yield the values shown in Table 4. Stronger evolution is found for both scenarios, when fitting the whole range of luminosities, which indicates that lower luminosity sources undergo less evolution than higher luminosity sources $\log_{10}L_{325MHz} > 24.5$ W Hz^{-1} a trend which has been seen by Waddington et al.
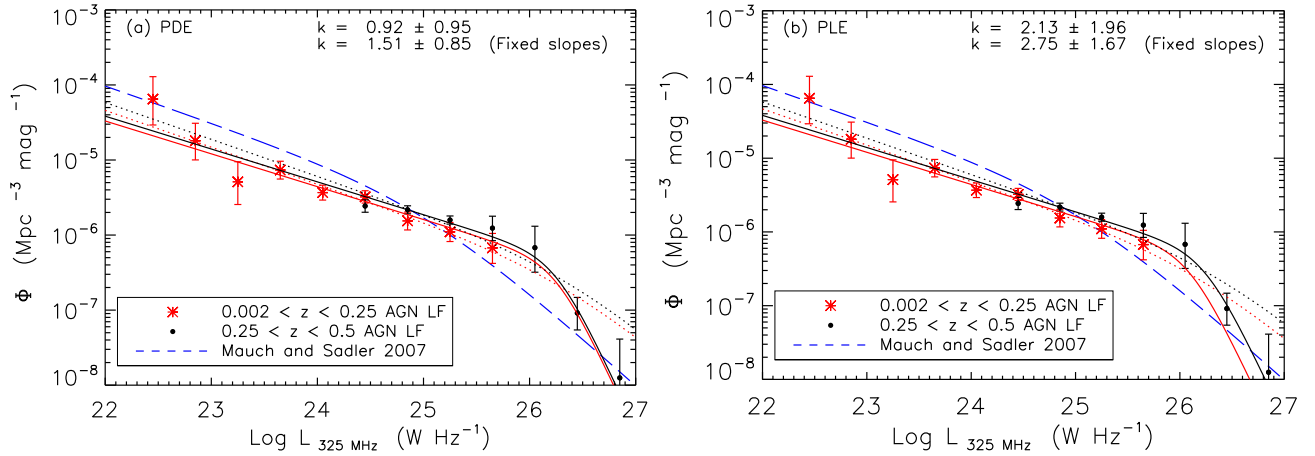
Figure 13. 325 MHz AGN RLFs for the redshift ranges $0.002 < z < 0.25$ (red crosses) and $0.25 < z < 0.5$ (black-filled circles). Panels (a) and (b) shows the best-fitting RLF assuming pure density and pure luminosity evolution respectively (solid lines). The best-fitting RLFs found by fixing the bright and faint-end slopes to be equal to those of Mauch & Sadler (2007) can be seen as dotted lines. The local RLF of Mauch & Sadler (2007), which has been converted to 325 MHz from 1.4 GHz assuming a spectral index of $\alpha = -0.7$ can be seen as a blue-dashed line. Bin sizes of $\Delta \log_{10} L = 0.4$ are used. Error bars are determined using the prescription of Gehrels (1986).

Table 2. The 325 MHz RLF for AGN.

Luminosity ($\log_{10}(L_{325MHz})$)	$0.002 < z < 0.25$ Number density (Mpc^{-3}mag^{-1})	Number	$0.25 < z < 0.5$ Number density (Mpc^{-3}mag^{-1})	Number
22.4	$6.49^{+6.41}_{-3.56} \times 10^{-5}$	3		
22.8	$1.81^{+1.28}_{-0.80} \times 10^{-5}$	5		
23.2	$5.12^{+4.36}_{-0.26} \times 10^{-6}$	4		
23.6	$7.35^{+2.27}_{-1.78} \times 10^{-6}$	19		
24.0	$3.68^{+0.93}_{-0.76} \times 10^{-6}$	26		
24.4	$3.22^{+0.67}_{-0.56} \times 10^{-6}$	35	$2.44^{+0.50}_{-0.42} \times 10^{-6}$	45
24.8	$1.54^{+0.48}_{-0.37} \times 10^{-6}$	19	$2.17^{+0.28}_{-0.25} \times 10^{-6}$	93
25.2	$1.10^{+0.36}_{-0.28} \times 10^{-6}$	15	$1.59^{+0.21}_{0.19} \times 10^{-6}$	83
25.6	$6.74^{+3.77}_{-2.55} \times 10^{-7}$	8	$1.24^{+0.55}_{-0.40} \times 10^{-6}$	47
26.0			$6.79^{+6.32}_{-3.59} \times 10^{-7}$	18
26.4			$9.13^{+5.62}_{-3.69} \times 10^{-8}$	6
26.8			$1.25^{+2.88}_{-1.04} \times 10^{-8}$	1
27.2			$1.25^{+2.88}_{-1.04} \times 10^{-8}$	1
Total		134		294

Table 3. Best-fitting parameters from fitting the 325 MHz RLF for pure luminosity and pure density evolution, assuming a double power law as in Dunlop et al. (1990). We fit the RLFs with and without fixing the power-law slopes as those found in Mauch and Sadler. (2007).

| Parameter	Evolution scenario PDE	PDE (Fixed slopes)	PLE	PLE (Fixed slopes)
$\log_{10}(L_*)$ W Hz^{-1}	26.26 ± 0.15	26.43 ± 0.51	25.96 ± 0.29	26.11 ± 0.52
$\log_{10}(C)$ Mpc^{-3}	-6.40 ± 0.19	-6.60 ± 0.27	-6.27 ± 0.15	-6.43 ± 0.26
A	3.08 ± 1.62	1.27 (Fixed)	3.02 ± 1.56	1.27 (Fixed)
B	0.44 ± 0.06	0.49 (Fixed)	0.44 ± 0.06	0.49 (Fixed)
k	0.92 ± 0.95	1.51 ± 0.92	2.13 ± 1.96	2.75 ± 1.51
Reduced χ^2	0.80	1.21	0.79	1.22

(2001), Willott et al. (2001), Tasse et al. (2008), Donoso, Best & Kauffmann (2009), Rigby et al. (2011), Simpson et al. (2012).

To investigate this further, we follow Clewley & Jarvis (2004) and calculate the parameter free V/V_{max} statistic as a function the

radio luminosity. The V in this case is the volume enclosed by the source at its true redshift and V_{max} is the volume up to which it could still be found given the survey parameters, i.e. the same V_{max} used to calculate the RLF. For a non-evolving population, then the radio

Table 4. Straight line of best-fitting parameters for the 325 MHz RLF assuming pure luminosity and pure density evolution for the whole range of luminosities and for AGN with $\log_{10}L_{325} < 25.5$ W Hz^{-1}.

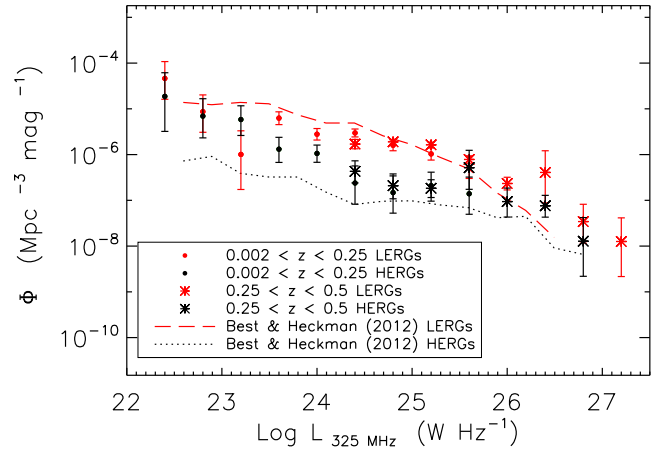| Parameter	PDE	PLE	PDE ($\log_{10}L_{325} < 25.5$ W Hz^{-1})	PLE ($\log_{10}L_{325} < 25.5$ W Hz^{-1})
			Evolution scenario	
m	-0.53 ± 0.05	-0.56 ± 0.04	-0.44 ± 0.06	-0.43 ± 0.06
c	7.28 ± 1.18	8.26 ± 1.06	5.21 ± 1.46	5.02 ± 1.43
k	1.46 ± 0.93	3.04 ± 1.48	0.81 ± 1.01	1.66 ± 2.13
Reduced χ^2	1.53	2.34	0.97	1.03
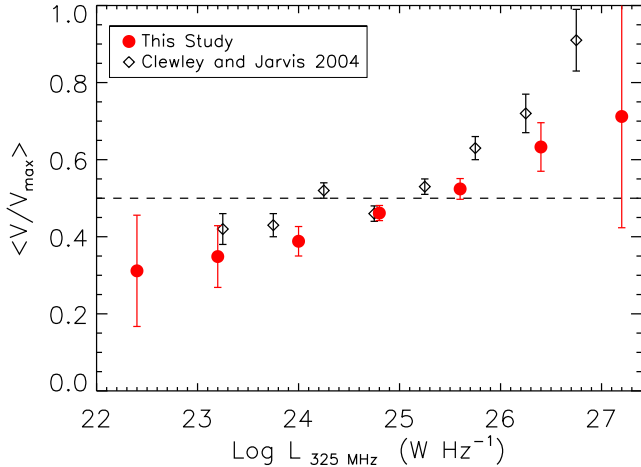
Figure 14. The V/V_{max} statistic as a function the radio luminosity for AGN out to $z = 0.5$ for the GMRT data (red circles), compared to the results of Clewley and Jarvis 2004 (black diamonds). Errors bars are given as $1/\sqrt{12N}$, as in Condon, Cotton & Broderick (2002).

Figure 15. RLFs for high (red data points) and low (black data points) excitation AGN in two redshift slices $0.002 < z < 0.25$ (filled circles) and $0.25 < z < 0.5$ (stars). The local 1.4 GHz HERG and LERG RLFs (converted to 325 MHz using a spectral indices of $\alpha = -0.7$) of Best and Heckman 2012, can be seen as the red-dashed and black-dotted lines, respectively.

sources should be uniformly distributed between 0 and 1 for this statistic, resulting in a constant comoving population giving a value of $V/V_{\mathrm{max}} = 0.5$, whereas a negatively evolving population would give $V/V_{\mathrm{max}} < 0.5$ and a positively evolving population resulting in $V/V_{\mathrm{max}} > 0.5$. Fig. 14 shows the V/V_{max} statistic for our sample, at radio luminosities $L_{325\mathrm{MHz}} < 10^{25}$ W Hz^{-1} the population does not appear to be evolving, whilst at $L_{325\mathrm{MHz}} > 10^{25}$ W Hz^{-1} there appears to be some evidence for positive evolution. At the faintest luminosities, it is possible that we do not see evolution due to the lack of volume probed. This is similar to what was found by Clewley & Jarvis (2004) albeit with a radio survey with a higher flux limit, and using photometric redshifts. Tasse et al. (2008) also show there is more positive evolution for radio-loud AGN with $L_{1.4\,\mathrm{GHz}} > 10^{24.5}$ W Hz^{-1} than at lower luminosities, consistent with the results here, using a sample of AGN observed at frequencies of 74, 230, 325 and 610 MHz using the VLA and GMRT in the *XMM*–LSS field.

6.4 High- and low-excitation AGN

The optical spectra allow us to separate the AGN population into HERGs and LERGs. As in Laing et al. (1994) and Best & Heckman (2012), we make use of the 5007 Å [O III] line to divide the HERG and LERG populations. Here, we define HERGs as those as having a measurable [O III] equivalent widths (EW) >5 Å, which results in a sample of 68 HERGs and 382 LERGs.

Fig. 15 shows the RLFs for HERGs and LERGs in two redshift slices $0.002 < z < 0.25$ and $0.25 < z < 0.5$, compared to the local 1.4 GHz HERG and LERG RLFs of Best & Heckman (2012) converted to 325 MHz, assuming a spectral index of $\alpha = -0.7$. A clear division between the HERG and LERG RLFs can be seen,

at luminosities between $10^{23} < L_{325\,\mathrm{MHz}} < 10^{26}$ W Hz^{-1}, and the LERGs are the dominant population. We calculate that the fraction of HERGs decreases from 0.3 between $0.002 < z < 0.25$ to 0.21 between $0.25 < z < 0.5$. The faint end and bright ends of the RLFs tend to converge. Comparing our results with those of Best & Heckman (2012), we find that the LERG RLFs agree well with each other, whereas the HERG RLFs tends to diverge at lower luminosities $L_{325\text{-}\mathrm{MHz}} < 10^{24}$ W Hz^{-1}.

As our sample size is small, we are unable to observe any evolution. Pracy et al. (submitted) will contain a detailed investigation of the evolution of HERGs and LERGs at 1.4 GHz, making use of GAMA redshifts, as well as a discussion of the divergence of the HERG RLFs at lower luminosities.

6.5 Steep- and flat-spectrum AGN

In the simplest form of the orientation-based unification of AGN, we expect the flat-spectrum sources to be a subset of the parent steep-spectrum population that happen to have their radio jets oriented along our line of sight (Urry & Padovani 1995). These flat-spectrum sources would therefore have their radio flux density boosted due to relativistic beaming effects, and their intrinsic luminosity could be significantly lower than observed.

One of the unique aspects of the 325 MHz data is that we have spectral indices for the entire sample of radio-loud AGN, therefore we are able to measure separable RLFs for AGN with steep ($\alpha < -0.5$) and flat ($\alpha > -0.5$) spectra. Fig. 16 shows the RLFs for the two populations for two different redshift slices; $0.002 < z < 0.25$ and $0.25 < z < 0.5$. The steep-spectrum sources are seen to
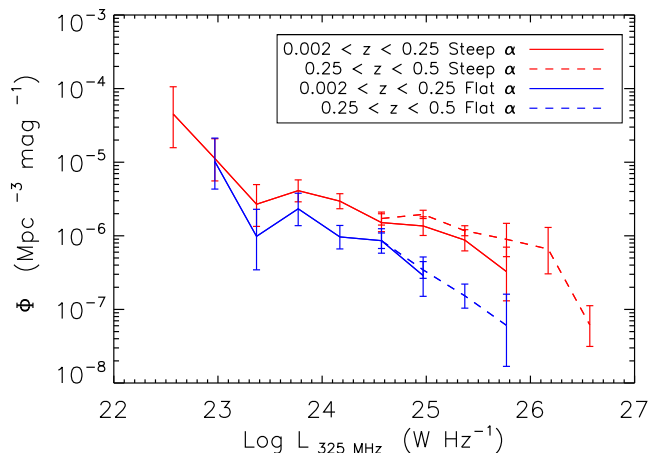
Figure 16. RLFs of AGN with steep ($\alpha < -0.5$, red) and flat ($\alpha > -0.5$, blue) spectral indices, for two redshift slices $0.002 < z < 0.25$ (solid lines) and $0.25 < z < 0.5$ (dashed lines).

Figure 17. Figure showing that the RLF (in the redshift slice $0.002 < z < 0.25$) for flat-spectrum sources (blue line) can be shifted in number density and luminosity (grey region), to coincide with an extrapolation of the steep-spectrum sources (red), as is expected from the orientation-based unification of radio-loud AGN.

be more numerous and span a wider range of luminosities than the flat-spectrum sources in our sample.

In order to determine whether the flat-spectrum objects are indeed a subset of the steep-spectrum sources, or conversely, we assume that they are and derive beaming parameters, to estimate the shift that is required on the flat-spectrum RLF for it to sit on the steep-spectrum RLF.

The radio flux density is enhanced as Γ^2:

$$\Gamma = \gamma^{-1}(1 - \beta \cos\theta)^{-1}, \tag{10}$$

where γ is the Lorentz factor, $\beta = v/c$ and θ is the angle between the radio jet and the line of sight. Following Jarvis & McLure (2002), we adopt a conservative approach and assume that the flat-spectrum population have an opening angle of $\theta \sim 20°$, which suggests a flux-boosting factor of the order of 10–20 over the steep-spectrum population. Furthermore, given the opening angle of $20°$, we can calculate the fraction of the parent population we are observing as flat-spectrum. Assuming a spherically symmetric system, then an opening angle of $20°$ corresponds to a fraction of 6 per cent of the parent population, from which we infer that the measured space density is a factor of $\sim$16 lower than it would be if we could see the unboosted population. To check if this is consistent with the RLF of the steep-spectrum sources, we shift the flat-spectrum RLF by a factor of 10 in luminosity, and a factor 16–20 in number density. Fig. 17 shows that this extrapolation of the steep-spectrum RLF (seen in grey) does indeed agree with the shifted RLF of the flat-spectrum population, as would be expected from orientation-based unification of radio-loud AGN. However, we have assumed that all of the flux from the flat-spectrum sources is Doppler boosted, whereas in reality some flux is undoubtedly emitted by extended jets or lobes which are not associated with the core of the radio sources. As such, our result that the flat-spectrum population forms a subset of the steep-spectrum population is only an indication that the orientation-based unification of radio-loud AGN is consistent with the data, rather than confirmation.

7 DISCUSSION

The results presented use data from a deep and wide 325 MHz survey from Mauch et al. (2013), combined with the optical imaging and spectroscopic redshifts from the GAMA survey. This sample is the
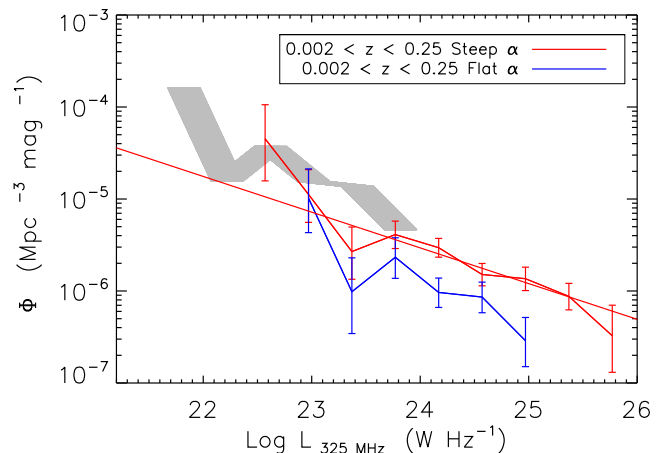
largest using spectroscopic redshifts obtained to date that spans a significant enough range in redshift ($0.002 < z < 0.5$) to measure evolution.

We find that the 325 MHz RLF for SF galaxies, at $z < 0.1$, is in agreement with those produced by combining 1.4 GHz NVSS and optical data from the 6dFGRS (Mauch & Sadler 2007). In order to determine a radio-derived estimate of the evolution of star formation rate density from the GAMA survey, we would require much deeper GMRT data going to lower flux limits. Padovani et al. (2011) for instance found that SF galaxies evolve as $L \propto (1+z)^{2.8}$, using 1.4 GHz data to flux limits of 50 μJy from the VLA-CDFS survey. Using 1.4 GHz VLA data matched to the VIDEO survey, McAlpine et al. (2013) found that the RLF of SF galaxies evolves as $L \propto (1+z)^{2.5}$, which is consistent with many other tracers of star formation (Hopkins et al. 2003; Hopkins 2004; Prescott, Baldry & James 2009).

Our measured 325 MHz RLF of AGN is in broad agreement with the 1.4 GHz RLF measured by Mauch & Sadler (2007) when converted to 325 MHz using a spectral index of $\alpha = -0.7$. The Mauch & Sadler (2007) LF also consistent with the local 20 GHz LF of Sadler et al. (2014), it therefore appears that the local AGN population is remarkably uniform over a large range in frequency (325 MHz to 20 GHz).

We note that, at the faint end, the 1.4 GHz RLF is consistently higher than our 325 MHz RLF, assuming the spectral index correction. The increased space density of 1.4 GHz selected galaxies may be due to Doppler boosting of the population, whereby beamed 1.4 GHz sources are shifted to higher luminosity. Radio-loud AGN samples selected at lower frequency are not as likely to detect significant numbers of sources with beamed cores, as at lower frequency the lobes of galaxies should dominate. This implies that the 325 MHz LFs presented here are not biased with respect to orientation and are more representative of the mechanical jet power in the local radio-loud AGN population.

Regarding evolution, we detect mild but poorly constrained evolution from fits to the 325 MHz RLF for AGN out to $z = 0.5$, with evolution parameters of $k = 0.92 \pm 0.95$ for pure density evolution and $k = 2.13 \pm 1.96$ for pure luminosity evolution. Considering just the low-luminosity population (those with $L_{325MHz} < 25.5$ W

Table 5. Comparison of the evolution parameters for radio-loud AGN determined from previous studies discussed above.

Study	Frequency	Flux limit	z Range	Sample size	Evolution parameter k	Redshifts
This study	325 MHz	∼5 mJy	$0.0 < z < 0.5$	428	2.13 ± 1.96 PLE	Spectro
					0.92 ± 0.95 PDE	
Brown et al. (2001)	1.4 GHz	5 mJy	$0.0 < z < 0.4$	230	3–5 PLE	Photo
Sadler et al. (2007)	1.4 GHz	2.8 mJy	$0.0 < z < 0.7$	391	2.3 ± 0.3 PLE	Spectro
Smolčić et al. (2009)	1.4 GHz	50 μJy	$0.0 < z < 1.3$	601	2.0 ± 0.3 PLE	Combined
McAlpine & Jarvis (2011)	1.4 GHz	1 mJy	$0.0 < z < 0.8$	131	0.8 ± 0.2 PLE	Photo
					0.6 ± 0.1 PDE	
Padovani et al. (2011)	1.4 GHz	50 μJy	$0.1 < z < 5.8$	86	-3.0 ± 1.0 PLE	Combined
					-1.6 ± 0.4 PDE	
McAlpine et al. (2013)	1.4 GHz	100 μJy	$0 < z < 2.5$	951	1.18 ± 0.21 PLE	Photo
Padovani et al. (2015)	1.4 GHz	50 μJy	$0.1 < z < 4.5$	136	-6.0 ± 1.4 PLE	Combined
					-2.4 ± 0.3 PDE	

Hz^{-1}) the evolution appears to be much less. This is in line with previous studies (see Table 5), principally based on smaller samples from deep fields, where the low-luminosity population evolves significantly less strongly that the high-luminosity population. Our results are also consistent with Donoso et al. (2009) and although they did not estimate an evolution parameter, they found that the number density of low-luminosity AGN increases by a factor of ∼1.5, out to $z = 0.55$, which implies an evolution parameter of $k \sim 0.93$.

Low-luminosity sources are thought to be the population that dominates the mechanical feedback in the $z < 1$ Universe (e.g. Croton et al. 2006; Smolčić 2009; Smolčić et al. 2009; Best & Heckman 2012; Smolcic et al. 2015), and thus constraining their evolution is key to our understanding of the relevance of such feedback in studies of galaxy evolution. However, we note that some fraction of such sources are thought to be powered by the efficient accretion of cold gas, determined by their emission-line properties (e.g. Simpson et al. 2012; Best et al. 2014; Mingo et al. 2014).

Historically, the vast majority of continuum surveys that have produced RLFs have been conducted at 1.4 GHz. Our result is in agreement with the only other comparable study concerned with the evolution of radio sources at 325 MHz by Clewley & Jarvis (2004), who by matching SDSS DR1 data with the WENSS, found no evolution in low-luminosity AGN via a V/V_{max} analysis, out to $z = 0.8$.

8 CONCLUSIONS

We have produced $1/V_{max}$ RLFs for samples of AGN and SF galaxies out to $z \sim 0.5$, by combining data from the largest survey conducted to date at 325 MHz from the GMRT, with the GAMA survey. Our main results are as follows:

(i) By cross-matching a 325 MHz GMRT survey covering 138 deg^2 of the GAMA spectroscopic survey, we are able to produce a GMRT/GAMA matched sample of 499 objects with $z \leq 0.6$, $nQ \geq 3$ and $r \leq 19.8$. Inspection of the optical spectra in our sample allows us to divide the sample into 45 SF galaxies and 453 AGN.

(ii) The mean spectral index of AGN remains constant with redshift as found in Smolčić et al. (2014, Fig. 8). Higher luminosity AGN are found to have slightly steeper spectral indices than those with lower luminosities possibly due to the increase in fraction of FR II sources (Fig. 9).

(iii) We determine the local luminosity function of SF galaxies at 325 MHz, which is broadly consistent with the local 1.4 GHz luminosity function of Mauch & Sadler (2007) converted to 325 MHz

assuming spectral index of $\alpha = -0.7$. We estimate that the lower limit on the local star formation rate density of the Universe is $\rho_{SFR} = 0.013 \pm 0.002$ M$_{\odot}$ yr^{-1} Mpc^{-3} (Fig. 12).

(iv) We determine RLFs of radio-loud AGN for two redshift slices. Fitting a double power mild evolution out to $z \sim 0.5$. Parametrizing the evolution as $\propto (1 + z)^k$, we find the best-fitting values $k = 0.92 \pm 0.95$ assuming pure number density and 2.13 ± 1.96 assuming the pure luminosity density (Fig. 13). From fitting single power-law functions to the RLFs, we show that low-luminosity sources evolve less than high-luminosity sources.

(v) We produce RLFs for the HERG and LERG populations of AGN. LERGs are the dominant population at luminosities between $10^{23} < L_{325MHz} < 10^{26}$. At higher luminosities, the space densities of the populations become comparable (Fig. 15).

(vi) After dividing the AGN sample into steep- and flat-spectrum sources, we show that the extrapolation of the steep-spectrum sources agrees with the shifted flat-spectrum, as expected from the orientation-based unification of radio-loud AGN (Fig. 17).

In order to fully understand the link between AGN-driven feedback and the shutting down or continuous quenching of star formation in galaxies, a full understanding of the link between radio power, accretion mode and environment as a function of redshift is required. In the near future, radio data obtained from the LOw-Frequency ARray (van Haarlem et al. 2013), the Australian Square Kilometre Array Pathfinder (ASKAP; Johnston et al. 2007) and MeerKAT (Jonas 2009), along with the VLA, will provide much greater sample sizes for AGN and SF galaxies allowing more stringent constraints on the evolution of the radio population, out to greater redshifts when combined with future spectroscopic surveys (e.g. Smith 2015). Eventually, the Square Kilometre Array will be used to study the evolution of AGN from the cosmic dawn (Smolcic et al. 2015). Further work using the GAMA data set will involve investigating the evolution of HERG and LERG populations of AGN at 1.4 GHz (Pracy et al. submitted).

VST KIDS, VISTA VIKING, *WISE*, Herschel-ATLAS, GMRT and ASKAP providing UV to radio coverage. GAMA is funded by the STFC (UK), the ARC (Australia), the AAO, and the participating institutions. The GAMA web site is http://www.gama-survey.org/

We acknowledge the IDL Astronomy User's Library, and IDL code maintained by D. Schlegel (IDLUTILS) as valuable resources.

We also thank the anonymous referee for their helpful comments which has improved the paper.

REFERENCES

Abazajian K. N. et al., 2009, ApJS, 182, 543
Allen S. W., Dunn R. J. H., Fabian A. C., Taylor G. B., Reynolds C. S., 2006, MNRAS, 372, 21
Baldry I. K., Glazebrook K., Brinkmann J., Ivezić Ž., Lupton R. H., Nichol R. C., Szalay A. S., 2004, ApJ, 600, 681
Baldry I. K. et al., 2010, MNRAS, 404, 86
Becker R. H., White R. L., Helfand D. J., 1995, ApJ, 450, 559
Bell E. F., 2003, ApJ, 586, 794
Best P. N., Heckman T. M., 2012, MNRAS, 421, 1569
Best P. N., Ker L. M., Simpson C., Rigby E. E., Sabater J., 2014, MNRAS, 445, 955
Bower R. G., Benson A. J., Malbon R., Helly J. C., Frenk C. S., Baugh C. M., Cole S., Lacey C. G., 2006, MNRAS, 370, 645
Brown M. J. I., Webster R. L., Boyle B. J., 2001, AJ, 121, 2381
Cannon R. et al., 2006, MNRAS, 372, 425
Clewley L., Jarvis M. J., 2004, MNRAS, 352, 909
Colless M. et al., 2001, MNRAS, 328, 1039
Condon J. J., 1989, ApJ, 338, 13
Condon J. J., 1992, ARA&A, 30, 575
Condon J. J., Cotton W. D., Greisen E. W., Yin Q. F., Perley R. A., Taylor G. B., Broderick J. J., 1998, AJ, 115, 1693
Condon J. J., Cotton W. D., Broderick J. J., 2002, AJ, 124, 675
Coppejans R., Cseh D., Williams W. L., van Velzen S., Falcke H., 2015, MNRAS, 450, 1477
Croton D. J. et al., 2006, MNRAS, 365, 11
Cruz M. J. et al., 2006, MNRAS, 373, 1531
Davis M. et al., 2003, in Guhathakurta P., ed, Proc. SPIE Conf. Ser. Vol. 4834, Discoveries and Research Prospects from 6- to 10-Meter-Class Telescopes II. SPIE, Bellingham, p. 161
De Breuck C. et al., 2001, AJ, 121, 1241
Donoso E., Best P. N., Kauffmann G., 2009, MNRAS, 392, 617
Driver S. P. et al., 2009, Astron. Geophys., 50, 5
Driver S. P. et al., 2011, MNRAS, 413, 971
Dunlop J. S., Peacock J. A., 1990, MNRAS, 247, 19
Evans D. A., Worrall D. M., Hardcastle M. J., Kraft R. P., Birkinshaw M., 2006, ApJ, 642, 96
Fabian A. C., 2012, ARA&A, 50, 455
Fan D., Budavári T., Norris R. P., Hopkins A. M., 2015, MNRAS, 451, 1299
Fanaroff B. L., Riley J. M., 1974, MNRAS, 167, 31P
Fernandes C. A. C. et al., 2015, MNRAS, 447, 1184
Franceschini A., Hasinger G., Miyaji T., Malquori D., 1999, MNRAS, 310, L5
Gehrels N., 1986, ApJ, 303, 336
Graham A. W., Scott N., 2015, ApJ, 798, 54
Gunawardhana M. L. P. et al., 2013, MNRAS, 433, 2764
Gunn J. E. et al., 1998, AJ, 116, 3040
Hardcastle M. J., Evans D. A., Croston J. H., 2007, MNRAS, 376, 1849
Heckman T. M., Best P. N., 2014, ARA&A, 52, 589
Hine R. G., Longair M. S., 1979, MNRAS, 188, 111
Hogg D. W., Finkbeiner D. P., Schlegel D. J., Gunn J. E., 2001, AJ, 122, 2129
Hopkins A. M., 2004, ApJ, 615, 209
Hopkins A. M., Beacom J. F., 2006, ApJ, 651, 142
Hopkins A. M. et al., 2003, ApJ, 599, 971
Hopkins A. M. et al., 2013, MNRAS, 430, 2047

Jackson N., Rawlings S., 1997, MNRAS, 286, 241
Jackson C. A., Wall J. V., 1999, MNRAS, 304, 160
James P. A., Knapen J. H., Shane N. S., Baldry I. K., de Jong R. S., 2008, A&A, 482, 507
Jarvis M. J., McLure R. J., 2002, MNRAS, 336, L38
Jarvis M. J., Rawlings S., 2000, MNRAS, 319, 121
Jarvis M. J., Rawlings S., Eales S., Blundell K. M., Bunker A. J., Croft S., McLure R. J., Willott C. J., 2001, MNRAS, 326, 1585
Jarvis M. J. et al., 2014, Proc. Advancing Astrophysics with the Square Kilometre Array (AASKA14). Available at: http://pos.sissa.it/cgi-bin/reader/conf.cgi?confid=215
Johnston S. et al., 2007, PASA, 24, 174
Jonas J. L., 2009, Proc. IEEE, 97, 1522
Jones D. H. et al., 2004, MNRAS, 355, 747
Kewley L. J., Dopita M. A., Sutherland R. S., Heisler C. A., Trevena J., 2001, ApJ, 556, 121
Kimball A. E., Knapp G. R., Ivezić Ž., West A. A., Bochanski J. J., Plotkin R. M., Gordon M. S., 2009, ApJ, 701, 535
Kormendy J., Richstone D., 1995, ARA&A, 33, 581
Laing R. A., Riley J. M., Longair M. S., 1983, MNRAS, 204, 151
Laing R. A., Jenkins C. R., Wall J. V., Unger S. W., 1994, in Bicknell G. V., Dopita M. A., Quinn P. J., eds, ASP Conf. Ser. Vol. 54, The Physics of Active Galaxies. Astron. Soc. Pac., San Francisco, p. 201
Lawrence A. et al., 2007, MNRAS, 379, 1599
Le Fèvre O. et al., 2005, A&A, 439, 845
Lilly S. J., Le Fevre O., Hammer F., Crampton D., 1996, ApJ, 460, L1
Lilly S. J. et al., 2007, ApJS, 172, 70
Liske J. et al., 2015, MNRAS, 452, 2087
Longair M. S., 1966, MNRAS, 133, 421
Loveday J. et al., 2015, MNRAS, 451, 1540
McAlpine K., Jarvis M. J., 2011, MNRAS, 413, 1054
McAlpine K., Smith D. J. B., Jarvis M. J., Bonfield D. G., Fleuren S., 2012, MNRAS, 423, 132
McAlpine K., Jarvis M. J., Bonfield D. G., 2013, MNRAS, 436, 1084
McAlpine K. et al., 2015, Proc. Advancing Astrophysics with the Square Kilometre Array (AASKA14). Available at: http://pos.sissa.it/cgi-bin/reader/conf.cgi?confid=215
Madau P., Dickinson M., 2014, ARA&A, 52, 415
Madau P., Ferguson H. C., Dickinson M. E., Giavalisco M., Steidel C. C., Fruchter A., 1996, MNRAS, 283, 1388
Magorrian J. et al., 1998, AJ, 115, 2285
Mauch T., Sadler E. M., 2007, MNRAS, 375, 931
Mauch T., Murphy T., Buttery H. J., Curran J., Hunstead R. W., Piestrzynski B., Robertson J. G., Sadler E. M., 2003, MNRAS, 342, 1117
Mauch T., Klöckner H.-R., Rawlings S., Jarvis M., Hardcastle M. J., Obreschkow D., Saikia D. J., Thompson M. A., 2013, MNRAS, 435, 650
Mingo B., Hardcastle M. J., Croston J. H., Dicken D., Evans D. A., Morganti R., Tadhunter C., 2014, MNRAS, 440, 269
Owen F. N., Morrison G. E., Klimek M. D., Greisen E. W., 2009, AJ, 137, 4846
Padovani P., Miller N., Kellermann K. I., Mainieri V., Rosati P., Tozzi P., 2011, ApJ, 740, 20
Padovani P., Bonzini M., Kellermann K. I., Miller N., Mainieri V., Tozzi P., 2015, MNRAS, 452, 1263
Prescott M., Baldry I. K., James P. A., 2009, MNRAS, 397, 90
Randall K. E., Hopkins A. M., Norris R. P., Zinn P.-C., Middelberg E., Mao M. Y., Sharp R. G., 2012, MNRAS, 421, 1644
Rengelink R. B., Tang Y., de Bruyn A. G., Miley G. K., Bremer M. N., Roettgering H. J. A., Bremer M. A. R., 1997, A&AS, 124, 259
Rigby E. E., Best P. N., Brookes M. H., Peacock J. A., Dunlop J. S., Röttgering H. J. A., Wall J. V., Ker L., 2011, MNRAS, 416, 1900
Robotham A. et al., 2010, PASA, 27, 76
Sadler E. M. et al., 2002, MNRAS, 329, 227
Sadler E. M. et al., 2007, MNRAS, 381, 211
Sadler E. M., Ekers R. D., Mahony E. K., Mauch T., Murphy T., 2014, MNRAS, 438, 796

Saripalli L., Hunstead R. W., Subrahmanyan R., Boyce E., 2005, AJ, 130, 896

Schmidt M., 1968, ApJ, 151, 393

Schoenmakers A. P., de Bruyn A. G., Röttgering H. J. A., van der Laan H., 2001, A&A, 374, 861

Sharp R. et al., 2006, in McLean I. S., Iye M., eds, Proc. SPIE Conf. Ser. Vol. 6269, Ground-based and Airborne Instrumentation for Astronomy. SPIE, Bellingham, p. 62690G

Shaver P. A., Wall J. V., Kellermann K. I., Jackson C. A., Hawkins M. R. S., 1996, Nature, 384, 439

Simpson C. et al., 2012, MNRAS, 421, 3060

Smith D. J. B., 2015, preprint (arXiv:1506.05630)

Smith D. J. B. et al., 2011, MNRAS, 416, 857

Smolcic V. et al., 2015, Proc. Advancing Astrophysics with the Square Kilometre Array (AASKA14). Available at: http://pos.sissa.it/cgi-bin/reader/conf.cgi?confid=215

Smolčić V., 2009, ApJ, 699, L43

Smolčić V. et al., 2009, ApJ, 696, 24

Smolčić V. et al., 2014, MNRAS, 443, 2590

Stoughton C. et al., 2002, AJ, 123, 485

Strateva I. et al., 2001, AJ, 122, 1861

Strauss M. A. et al., 2002, AJ, 124, 1810

Sutherland W., Saunders W., 1992, MNRAS, 259, 413

Tasse C., Best P. N., Röttgering H., Le Borgne D., 2008, A&A, 490, 893

Taylor E. N. et al., 2011, MNRAS, 418, 1587

Urry C. M., Padovani P., 1995, PASP, 107, 803

van Haarlem M. P. et al., 2013, A&A, 556, A2

Waddington I., Dunlop J. S., Peacock J. A., Windhorst R. A., 2001, MNRAS, 328, 882

Wall J. V., Jackson C. A., Shaver P. A., Hook I. M., Kellermann K. I., 2005, A&A, 434, 133

Westra E., Geller M. J., Kurtz M. J., Fabricant D. G., Dell'Antonio I., 2010, ApJ, 708, 534

Willott C. J., Rawlings S., Blundell K. M., Lacy M., Eales S. A., 2001, MNRAS, 322, 536

York D. G. et al., 2000, AJ, 120, 1579

This paper has been typeset from a TEX/LATEX file prepared by the author.